









# Deletion of *Mocos* Induces Xanthinuria with Obstructive Nephropathy and Major Metabolic Disorders in Mice

Delphine Sedda,<sup>1</sup> Claire Mackowiak <sup>1</sup>, Julie Pailloux,<sup>1</sup> Elodie Culerier,<sup>1</sup> Ana Dudas <sup>1</sup>, Pauline Rontani,<sup>2</sup> Nicolas Erard,<sup>2</sup> Antoine Lefevre,<sup>3</sup> Sylvie Mavel <sup>3</sup>, Patrick Emond <sup>3,4,5</sup>, Frederic Foucher <sup>6</sup>, Marc Le Bert <sup>1</sup>, Valerie F.J. Quesniaux <sup>1</sup>, Michael J. Mihatsch,<sup>7</sup> Bernhard Ryffel,<sup>1</sup> and Madeleine Erard-Garcia <sup>1</sup>

## Key Points

- A knockout mouse targeting the molybdenum cofactor sulfurase (*Mocos*) gene develops xanthinuria type II with lethal obstructive nephropathy.
- Xanthinuric *Mocos* knockout mice display moderate renal inflammation and fibrosis, normocytic anemia, and reduced detoxification defense systems.
- Purine, but also amino acid and phospholipid, metabolic pathways are altered in *Mocos* knockout kidneys.

## Abstract

**Background** Xanthinuria type II is a rare autosomal purine disorder. This recessive defect of purine metabolism remains an under-recognized disorder.

**Methods** Mice with targeted disruption of the molybdenum cofactor sulfurase (*Mocos*) gene were generated to enable an integrated understanding of purine disorders and evaluate pathophysiologic functions of this gene which is found in a large number of pathways and is known to be associated with autism.

**Results** *Mocos*-deficient mice die with 4 weeks of age due to renal failure of distinct obstructive nephropathy with xanthinuria, xanthine deposits, cystic tubular dilation, Tamm–Horsfall (uromodulin) protein (THP) deposits, tubular cell necrosis with neutrophils, and occasionally hydronephrosis with urolithiasis. Obstructive nephropathy is associated with moderate interstitial inflammatory and fibrotic responses, anemia, reduced detoxification systems, and important alterations of the metabolism of purines, amino acids, and phospholipids. Conversely, heterozygous mice expressing reduced MOCOS protein are healthy with no apparent pathology.

**Conclusions** *Mocos*-deficient mice develop a lethal obstructive nephropathy associated with profound metabolic changes. Studying MOCOS functions may provide important clues about the underlying pathogenesis of xanthinuria and other diseases requiring early diagnosis.

KIDNEY360 2: 1793–1806, 2021. doi: <https://doi.org/10.34067/KID.0001732021>

## Introduction

Xanthinuria is a rare hereditary disorder of purine metabolism. Two forms can be distinguished: classic xanthinuria type I, caused by xanthine dehydrogenase (XDH) deficiency alone; and xanthinuria type II, caused by the dual deficiency of XDH and aldehyde oxidase 1 (AOX1), two enzymes whose activity depends on the presence of molybdenum cofactor sulfurase (MOCOS). Both forms are autosomal recessive disorders displaying identical clinical phenotypes. In

about two thirds of affected individuals, xanthinuria remains an asymptomatic metabolic abnormality throughout life. In the remaining third, xanthine stones form and lead to varying degrees of nephrolithiasis, hydronephrosis, and—in some cases—renal failure (1). Clinically, both forms are characterized by marked depletion of uric acid and accumulation of xanthine in blood and urine. Other less common manifestations linked to xanthine deposits may develop, such as myositis, arthropathy, and duodenal ulcer (2).

<sup>1</sup>Experimental and Molecular Immunology and Neurogenetics (INEM), Orléans University, Centre National de la Recherche Scientifique (CNRS) UMR7355, Orléans, France

<sup>2</sup>Institute of NeuroPhysiopathology (INP), Aix-Marseille University, CNRS UMR7051, Marseille, France

<sup>3</sup>iBrain, Tours University, Institut National de la Santé et de la Recherche Médicale (INSERM) UMR 1253, Tours, France

<sup>4</sup>Division of In Vitro Nuclear Medicine, Regional University Hospital of Tours, Tours, France

<sup>5</sup>PST Analysis of Biological Systems, Tours University, Tours, France

<sup>6</sup>Center for Molecular Biophysics (CBM), CNRS UPR4301, Orléans, France

<sup>7</sup>Institute for Pathology, University Hospital of Basel, Basel, Switzerland

**Correspondence:** Dr. Madeleine Erard-Garcia, INEM, CNRS UMR7355, 3B, Rue de la Férollerie, 45071 Orléans CEDEX 2, France.  
E-mail: [madeleine.erard@cnrs-orleans.fr](mailto:madeleine.erard@cnrs-orleans.fr)

The differential diagnosis between type I and type II classic xanthinuria relies on a detailed medical history and the response to allopurinol in patients who are hypouricemic, with patients who have xanthinuric type II failing to metabolize allopurinol into oxypurinol (3).

To date, the true incidence and prevalence of classic xanthinuria is unknown because it is rarely reported, often not recognized, and is underexplored. In this context, only a few cases of xanthinuria type II caused by point mutations in the coding sequence of *MOCOS* have been reported in humans (4–9). *MOCOS* encodes a ubiquitous enzyme that catalyzes the insertion of a terminal sulfur ligand onto the molybdenum cofactor (MOCO), converting the oxo form of MOCO into a sulfurated form (10). The structure of the mammalian *MOCOS* is similar to ABA3, its plant homolog: it is a two-domain protein containing an amino-terminal domain, which shows homologies to L-cysteine desulfurase, and a carboxy-terminal domain, which is able to bind MOCO (11–13). After sulfuration by *MOCOS*, sulfurated-MOCO is required to activate XDH and AOX1, two structurally complex oxidoreductases. XDH is a rate-limiting enzyme in the oxidative metabolism of purines: it allows the conversion of hypoxanthine and xanthine to uric acid and the oxidation of allopurinol to oxypurinol (14). XDH is thought to play a key role in a variety of physiologic, but also pathophysiologic, conditions, such as ischemia-reperfusion injury, endothelial dysfunction, and diabetes mellitus, but also cardiovascular diseases, renal failure, and cancer (15). XDH is also a significant component of innate inflammatory signaling and a major source of reactive oxygen species (ROS) (16). Conversely, little is known about the physiologic relevance of AOX1, except that it catalyzes the oxidation of several aldehydes to their cognate acids (17). As XDH, AOX1 is a critical source of ROS and nitric oxide (NO), and it is increasingly recognized as a major contributing factor to drug metabolism and as a source of ROS possibly involved in human pathology (18,19).

No studies on the potential effect of *MOCOS* deletion on kidney function, and the mechanism by which such mutation could contribute to xanthinuria, have been performed. In addition, *MOCOS* alterations may cause genetic damage on their own and orchestrate a wide variety of clinical syndromes. *MOCOS* deficiency might be regarded as a risk factor in autism spectrum disorders (ASD), disrupting the oxidative stress response and synaptogenesis in neurons derived from human induced pluripotent stem cells (20–22). Although these findings indicate that *MOCOS* serves important functions in tissue homeostasis and during neuronal development, the reasons for the wide range of pathophysiologic phenotypes observed in *MOCOS* deficiencies are unclear. To gain insights into the role of *MOCOS* in purine metabolism and as-yet-unidentified pathways, we have analyzed a new mouse model knockout (KO) for *Mocos*.

We show here that *Mocos* KO mice die within 4 weeks with xanthinuria and renal failure. Whereas heterozygous *Mocos* mice grow normally into apparently healthy, fertile adults, *Mocos* KO mice develop obstructive nephropathy with xanthine deposits. In xanthinuric mice, reduced antioxidant defense systems, along with anemia, may also be involved in the progression of renal injury. Finally, consistent with a role of *MOCOS* in various signaling pathways,

we also report major differences of metabolism between kidneys of *Mocos* KO and littermate wild-type mice, which are related to purine, but also amino acid and phospholipid, metabolic pathways. These observations suggest that, in addition to its role in purine metabolism leading to obstructive nephropathy, *MOCOS* deficiency has as-yet-unknown functions in other metabolic processes.

## Materials and Methods

### Generation of *Mocos*<sup>em2(IMPC)ics</sup> KO Mice and Animal Matings

The CRISPR/Cas9 system was used to generate mice with complete *Mocos* KO by zygotic injection of CAS9 and multiple adjacent single-guide RNAs that target exon 3. Genome editing was performed at the PHENOMIN Mouse Clinical Institute (ICS; Strasbourg, France). The conditions used at ICS to generate the *Mocos* KO *via* the CRISPR/Cas9 approach can be found at <http://www.ics-mci.fr/>.

The PHENOMIN project received approval from ethics committees and authorization from the French Ministry of Research. The project was evaluated taking the 3Rs (replace, reduce, and refine) and harm-benefit analysis concepts into account, with a focus on refinement (use of anesthesia, of painkillers when needed, respect of good practices).

The specific primer sequences used for genotyping were as follows:

*Mocos* forward, GGGGATTGTTGTATTGTGCCTGTCTG;  
*Mocos* reverse, CTTGCCCTCTGTCTTCTGACCTGAGG.

*Mocos* KO mice were obtained by crossing mice heterozygous for the gene *Mocos*. Experiments were performed with 4- to 10-week-old female or male mice. All *Mocos*-deficient mice and wild-type littermate controls (C57BL/6J background) were bred and housed in our specific pathogen-free animal facility at TAAM (Transgenesis, Archiving and Animal Models, TAAM-UPS 44, CNRS, Orléans, France) under agreement D-45-234-6, 2014. Mice were maintained in a temperature-controlled (23°C) facility, with strict 12-hour light/dark cycles, and were given free access to food and water. Animal experiments were performed in accordance with the French Institutional Committee under agreement CLE CCO 2017-1134.

### Hematology and Urine Analysis

Blood was collected in EDTA tubes (20.1341.100; Sarstedt) and read with the SCIL Vet abc Plus analyzer. Before use, serum was collected in Microvette gel tubes (20.1344; Sarstedt) and centrifuged at 10000 × g for 5 minutes. Xanthine/hypoxanthine levels were determined using the Xanthine/Hypoxanthine Assay Kit (ab155900; Abcam) following the manufacturer's protocol. Urine was freshly collected and pH was determined using pH indicator paper (2600 108; Whatman).

### Histologic and Immunofluorescence Analysis

Dissected tissues were fixed in 4% buffered paraformaldehyde (PFA) and paraffin embedded under standard conditions. Tissue sections (3 μm) were stained with hematoxylin and eosin and special stains according to standard

laboratory procedures. Immunohistochemistry for uromodulin/THP was performed according to standard procedures (<https://esp-nephropathology-working-group.org/technical-notes/>) using a mouse mAb purchased from Cedarlane.

For immunofluorescence, tissues were fixed for 3 days in 4% PFA and submerged in 20% sucrose for 1 week. They were then embedded in optimal cutting temperature compound (Tissue-Tek) and 10  $\mu$ m sections were prepared with a cryotome (Leica). Terminal deoxynucleotidyl transferase-mediated digoxigenin-deoxyuridine nick-end labeling staining was performed on sections using the ApopTag Fluorescein *In Situ* Apoptosis Detection Kit (S7110; Merck), following the manufacturer's protocol. For Ki67 (PCNA) staining, slides were incubated for 30 minutes in citrate buffer at 80°C, washed in Tris-buffered saline/Tween 20, and then incubated overnight with rabbit anti-mouse Ki67 (4  $\mu$ g/ml, ab15580; Abcam). After washing, slides were treated with 0.05% pontamine sky blue (Sigma) for 15 minutes and then incubated with secondary goat anti-rabbit antibody (2  $\mu$ g/ml, ab150077; Abcam) for 45 minutes at room temperature. After washing, slides were incubated with 4',6-diamidino-2-phenylindole (Fisher Scientific) and mounted in Fluoromount-G (SouthernBiotech). Tissue sections were analyzed on a Leica fluorescence microscope (CTR6000) at  $\times$ 200 magnification. The slides were analyzed and semiquantitatively scored (Supplemental Methods, Histological and immunofluorescence Analysis).

#### RNA Preparation, PCR, and Quantitative PCR

Total RNA was extracted using TRI-Reagent (Sigma) according to the manufacturer's instructions. RNA integrity and quality were controlled using Agilent RNA 6000 Nano Kit. Reverse transcription was performed with the SuperScript III Kit (Invitrogen), and the resultant cDNA was quantitatively amplified with real-time PCR using the QuantiTect Primer Assay kit (Qiagen) and GoTaq qPCR Master Mix (Promega). RNA expression was normalized to TATA-binding protein expression, and data were analyzed using the comparative analysis of relative expression by  $\Delta\Delta$ Ct methods. Primers sequences are reported in Supplemental Table 1.

#### Western Blot

Protein concentrations were quantified using the Bio-Rad DC Protein Assay Kit following the manufacturer's instructions. After blocking, membranes were probed with rabbit anti-MOCOS (1:100, NBP2-14243; Novus Biologicals), rabbit anti-AKR1C1 (1:1000, 105620, GeneTex), or mouse anti- $\beta$ -actin (1:5000, A2228, Sigma-Aldrich) antibodies. After overnight incubation at 4°C, the appropriate horseradish peroxidase-conjugated secondary IgG antibodies were added for 2 hours at room temperature. Signals were quantified using ImageJ software.

#### Metabolic Analysis

Metabolic analyses were performed by liquid chromatography coupled with high-resolution mass spectrometry, using standard metabolomics approaches (23,24). Briefly, frozen kidney tissue samples were lyophilized for 48 hours and milled to a fine powder. Ground samples (2 mg) were

extracted with 1.5 ml of methanol/MilliQ water (1:1). After centrifugation, the supernatants were collected and concentrated at 35°C for 2.5 hours. Analyses were done on a UPLC Ultimate 3000 System (Dionex) coupled to a Q-Exactive Mass Spectrometer (Thermo Fisher Scientific, Dreieich, Germany) and operated in positive and negative electrospray ionization modes. Chromatography was carried out using a Phenomenex Kinetex 1.7 mXB-C18 (150 mm $\times$ 2.10 mm) and 100 Å ultra high performance liquid chromatography column. The solvent system comprised mobile phase A (0.5% vol/vol formic acid in water), and mobile phase B (0.5% vol/vol formic acid in methanol). Data were processed using Xcalibur software (Thermo Fisher Scientific, San Jose, CA). A library of standard compounds (Mass Spectroscopy Metabolite Library of Standards supplied by IROA Technologies) were analyzed with the same conditions and gradient of mobile phases as those used to analyze the extracted metabolites. For data processing, briefly, peaks with >30% variance in quality-control samples were removed. The normalization was applied to the total area of the peaks of interest. Multivariate analyses were performed using SIMCA-P+ 15 software (Umetrics, Umeå, Sweden), as previously described (25). Briefly, the data analyses were first conducted using principal component analysis to detect outliers. Discriminant metabolites were obtained after orthogonal partial-least-squares discriminant analysis, after elimination of metabolites with low effect in the separation of the different groups. The listing of discriminant metabolites (very important in projection) is given in Supplemental Table 2. Univariate analyses were performed as nonparametric tests (Wilcoxon rank-sum test) using the free server MetaboAnalyst<sup>52</sup> (<https://www.metaboanalyst.ca/>) with a false discovery rate-adjusted *P* value of 0.05.

#### Statistical Analysis

All values were presented in the form of mean $\pm$ SEM. Statistical evaluation of differences between the experimental groups was done using the Mann-Whitney nonparametric test or log rank test for survival. All tests were performed using GraphPad Prism (GraphPad Software Inc., San Diego, CA; [www.graphpad.com](http://www.graphpad.com)). A *P* value <0.05 was considered significant.

## Results

### Mice Containing a Null Mutation of *Mocos* Induces a Partial Lethal Phenotype and Die Prematurely

To characterize the physiologic role of *Mocos*, mice with a targeted disruption in the *Mocos* locus were generated using CRISPR/Cas9 genome-editing technology (Figure 1A). After validation of the deletion by sequencing, a significant reduction of *Mocos* mRNA and MOCOS protein levels further confirmed targeting of the gene in engineered mice. Transcript level and protein concentration were reduced to roughly half in heterozygous *Mocos*<sup>+/-</sup> mice (Figure 1, B and C).

Mice homozygous for the disrupted *Mocos* gene were born phenotypically normal (Figure 1D), but only a few mice were recovered at weaning, pointing toward late embryonic or perinatal lethality. Further analysis showed

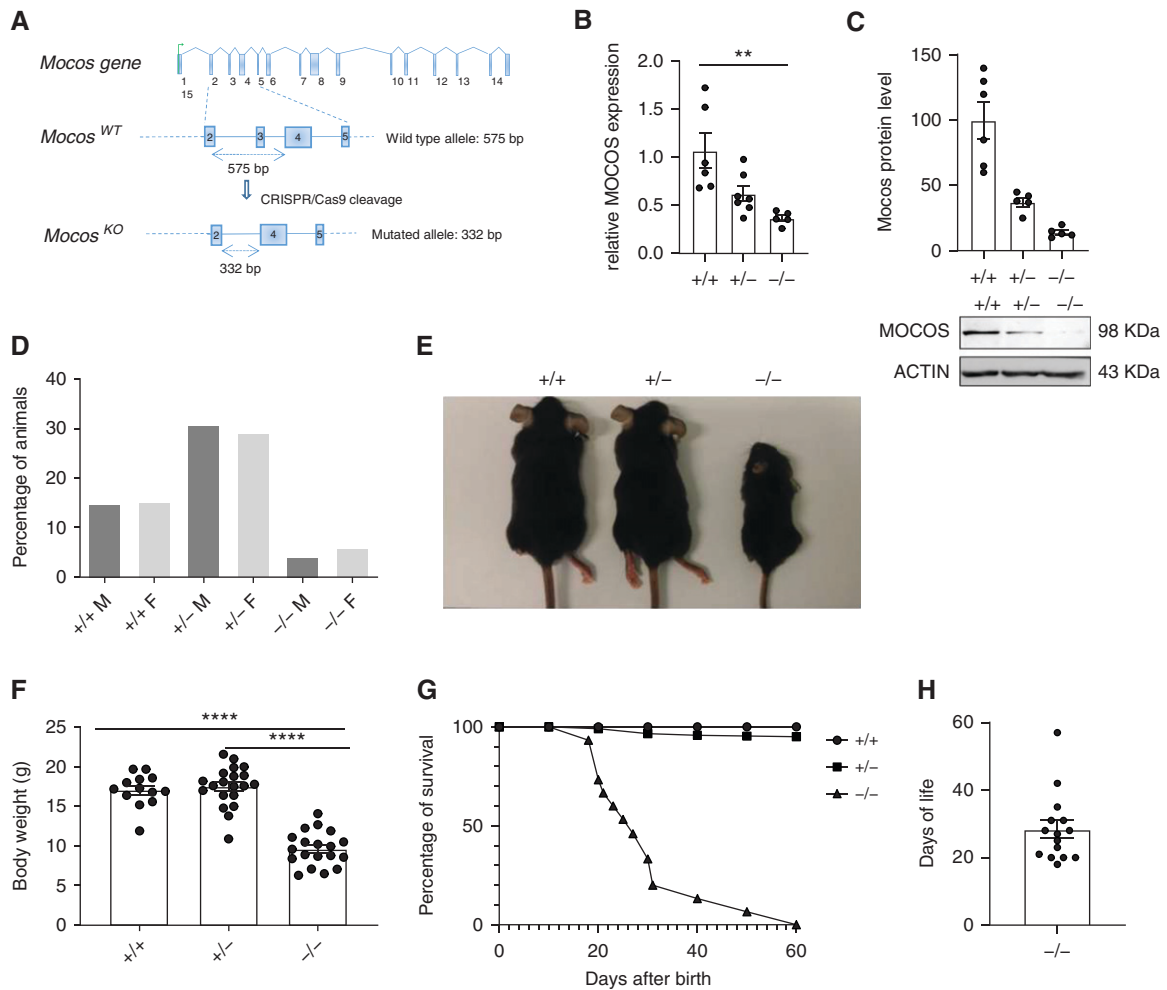


**Figure 1. | Knockout of *Mocos* induces a partial phenotype in mice.** (A) Schematic representation of the molybdenum cofactor sulfuryase (*Mocos*) disruption strategy using CRISPR/Cas9 technology. The deletion of exon 3 induces the loss of reading frame when splicing between exon 2 and exon 4, resulting in a truncated, nonfunctional MOCOS protein. (B) Relative *Mocos* expression was quantified by quantitative PCR. Data were from mice at 4 weeks of age and are expressed as mean ± SEM. (C) Renal expression and quantification of MOCOS protein by Western blot (data were from 4-week-old animals). (D) Frequency distribution of animals of the indicated genotype. The percentages of male and female mice of each genotype are indicated. (E) Phenotypic comparison of wild-type<sup>+/+</sup>, heterozygous *Mocos*<sup>+/-</sup>, and knockout (KO) *Mocos*<sup>-/-</sup> mice. *Mocos*<sup>-/-</sup> animals are easily distinguished from littermates at 4 weeks because of their reduced body size and weight. (F) Body weight of mice at 4 weeks of age; 12–17 animals per group were analyzed. Data are expressed as mean ± SEM. (G) Percentage of survival of wild-type (circle, n=168), heterozygous (square, n=239), and *Mocos*<sup>-/-</sup> (triangle, n=15) mice in days after birth. (H) Life span of *Mocos*<sup>-/-</sup> mice (n=15). M, male; F, female; WT, wild-type. \*\*P < 0.01, \*\*\*\*P < 0.0001.

there was an increased frequency of dead pups after birth, although the exact frequency cannot be determined due to cannibalization by the mother. These findings indicate a high perinatal mortality of homozygous pups. Young *Mocos*<sup>+/-</sup> mice were easily recognized from littermate controls after the first 2 weeks of life when they stopped gaining weight (Figure 1, E and F). Shortly thereafter, all *Mocos* KO mice died between 3–8 weeks of age, with an average life span of 28.4 days (Figure 1, G and H). In contrast, heterozygous mice were not different from wild-type mice derived from heterozygous breeding pairs; the mice survived and developed normally into apparently healthy, fertile adults (Supplemental Figure 1A). These observations indicated that the *Mocos* deficiency in the mouse leads to a lethal phenotype with incomplete penetrance and

premature death. Because of the runt appearance of the *Mocos* KO mice, all subsequent analyses were conducted on *Mocos* KO mice before death between 3 and 4 weeks of age. In addition, we closely monitored heterozygous mice for possible signs of disease in adult animals for a prolonged period ranging from 2 to 20 months of age.

#### Inactivation of *Mocos* Causes Abnormal Morphologic Features

At 4 weeks of age, *Mocos*-deficient mice displayed major morphologic abnormalities with significant reductions in kidney/body weight and liver/body weight ratios (33% and 20% reduction, respectively) and a substantial increase in brain/body weight ratios (51% increase) when compared with organ/body weight sizes of littermate controls



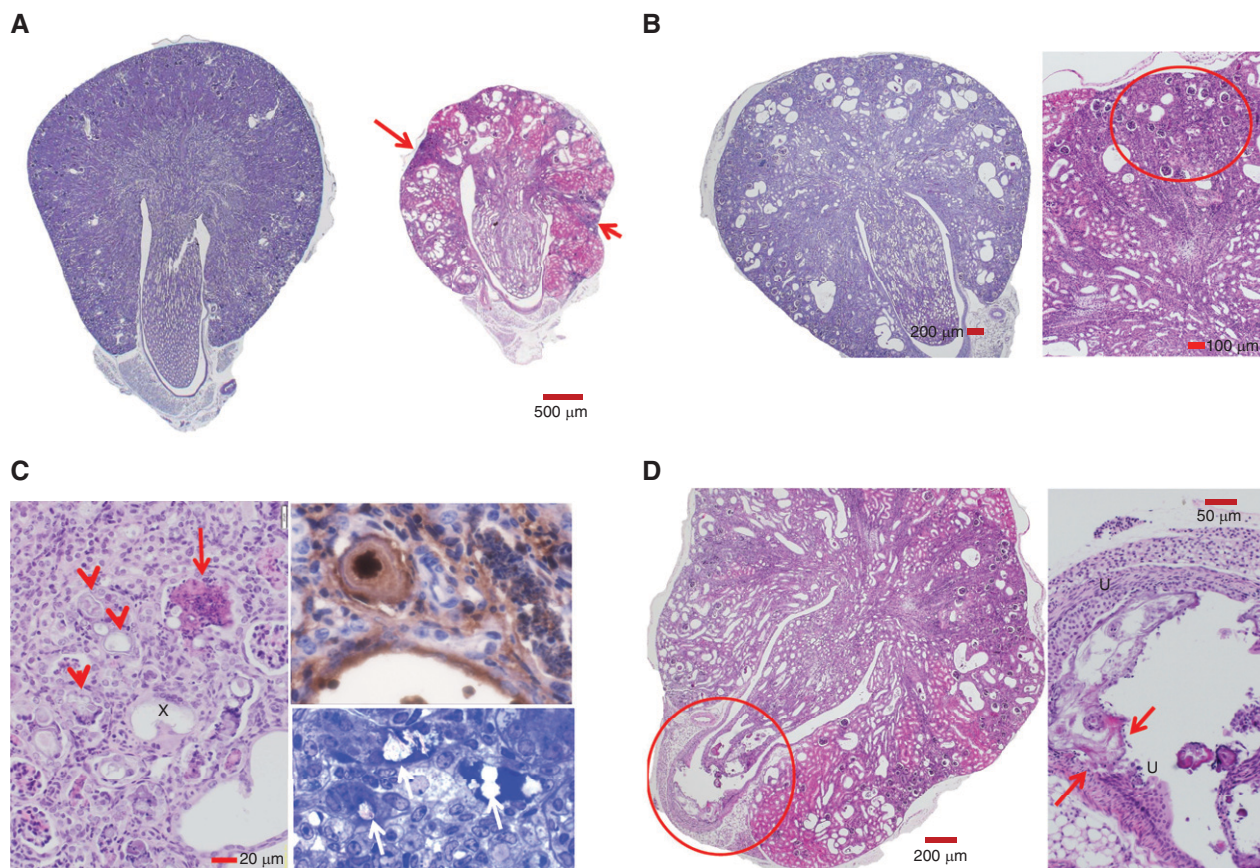


**Figure 2. | *Mocos* knockout induces obstructive nephropathy.** (A) Representative images of whole kidney sections of mice at the age of 4 weeks. KO kidney shows an irregular outer contour due to numerous scars (indentions, arrows) and cystoid tubules (right, hematoxylin and eosin [H&E] stain). Control kidney (left, trichrome stain). By planimetry, the size of the KO kidneys was reduced by 50% on average. (B) KO mouse: prominent interstitial fibrosis (blue staining cortex, trichrome stain) and numerous cystoid tubules, mainly cortical collecting ducts (left), subcapsular scar with densely packed glomeruli (encircled), interstitial fibrosis, and scanty interstitial infiltrates (right, H&E stain). (C) Tubulointerstitial space with dilated tubules, some with PMNs (arrow) or lamellate bodies (uromodulin, arrowheads), intratubular giant cell (X) and loss of tubular epithelium (left, H&E stain). Right top: lamellate roundish intratubular deposit (stained for uromodulin with immunohistochemistry, brown); note the adjacent tubule stuffed full with PMNs. Right bottom: Empty crystal clefts in tubules (arrow, semithin section stained with methylene blue). (D) Kidney cross-section similar to (A) and (B). Papillary tip on the opposite side renal pelvis covered by uromodulin. The ducts in the papillary tip are highly dilated and contain lamellate bodies (left, H&E stain). Right higher magnification of the pelvic wall; note the damage of the urothelium with denudation (between arrows) of the pelvic smooth muscle wall (arrow). The adjacent urothelium is preserved (U).

(Supplemental Figure 1, B–E). No significant differences in the size or gross morphology in all other organs, including lung, spleen, or intestine, were observed (Supplemental Figure 1, F–H). In contrast, *Mocos* heterozygotes showed normal proportions of all organs, except the liver, which showed a 21% reduction in liver/body weight size when compared with young wild-type mice (Supplemental Figure 1, B–H).

#### ***Mocos* KO Mice Develop Obstructive Nephropathy**

Anatomic examination of *Mocos*<sup>-/-</sup> mice revealed that all internal organs appeared grossly normal with the exception of the kidneys. Macroscopically, the mutation produces profound modifications of the renal structure: kidneys were pale, reduced in size, and with an irregular surface; whereas heterozygous *Mocos*<sup>+/-</sup> mice and wild-type littermates appeared normal (Supplemental Figure 1, B and C).

At low-power magnification, the histologic evaluation of *Mocos* KO kidneys displayed three major lesions: (1) cystic dilation of tubules, mainly in the cortex and less in the medulla (Figure 2A); (2) intratubular deposits of round lamellate deposits of THP with occasionally embedded crystals (empty crystal clefts, Figure 2, C and D); and (3) THP deposits in the renal pelvis with damage of the urothelium, accompanied by inflammation in the surrounding tissue. In the dilated and nondilated collecting ducts, round lamellate deposits of THP were present (Figure 2C). These deposits often displayed a basophilic rim—suggestive of calcification—but had negative von Kossa staining and no birefringent crystals were found after PFA fixation. However, few empty crystal clefts were present (Figure 2C). The adjacent epithelium was flattened or necrotic with intraluminal cell debris containing neutrophils and a few multinucleated giant cells surrounding the deposits (Figure 2C). The interstitial space

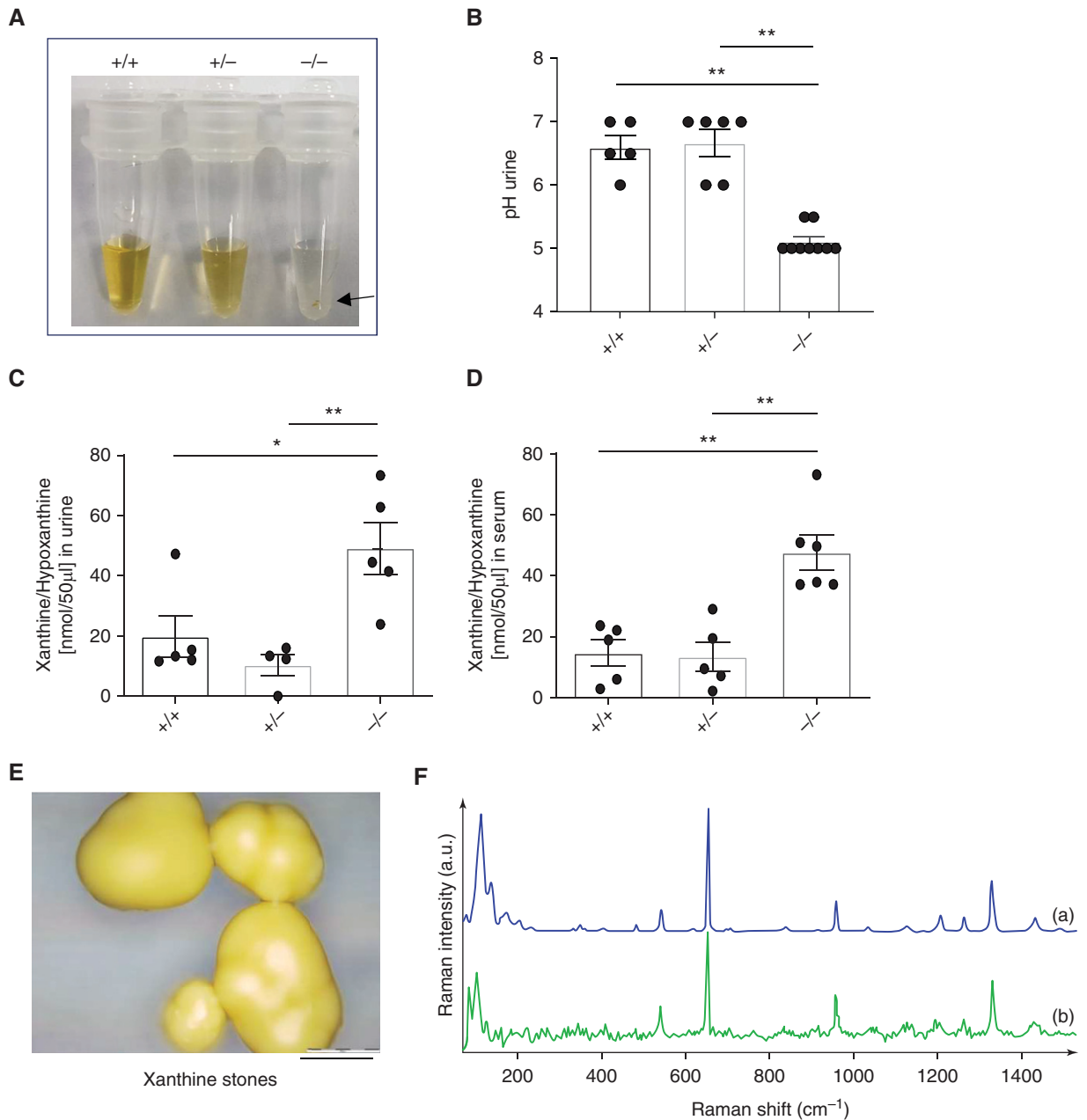


**Figure 3. | Constitutive *MOCOS* KO mice accumulate xanthine stones.** (A) The picture shows representative images of the transparent urine of homozygous *Mocos*<sup>-/-</sup> mice compared with the yellow color of urine characterizing wild-type and heterozygous *Mocos*<sup>+/-</sup> mice. The arrow points to deposits in urine from a *Mocos*<sup>-/-</sup> mouse. (B) Measurement of urinary pH in mouse strains. Data were from mice at 4 weeks of age and are expressed as mean±SEM. (C) Concentrations of xanthine and hypoxanthine are significantly increased in urine and (D) serum of homozygous *Mocos*<sup>-/-</sup> mice compared with age-matched littermate controls. Data were from mice at 4 weeks of age and are expressed as mean±SEM. (E) The picture is an example of xanthine stones from a *Mocos*<sup>-/-</sup> mouse. Scale bar, 200 µm. (F) Crystals collected from a *Mocos*<sup>-/-</sup> kidney were analyzed by Raman spectroscopy. In these crystals, the strongest bands observed at 542, 653, 960, 1208, 1264, 1330 and 1433 cm<sup>-1</sup> are considered as marker bands of xanthine (lower green panel) by comparison with a commercial standard (upper blue panel). \**P*<0.05, \*\**P*<0.01.

was slightly edematous and, adjacent to dilated collecting ducts, cortical areas displayed tubular atrophy, interstitial fibrosis, and mononuclear cell infiltrates (predominately in the subcapsular area; Figure 2, B–D). Primary lesions in glomeruli and vessels were not found. In areas of tubular atrophy, the glomeruli lay close together, varied in size, had collapsed capillary loops, and were very rarely

sclerotic. Moreover, some deposits of THP, similar to those present in the collecting ducts, were also found in the renal pelvis. These deposits were adhering to the urothelium, giving rise to urothelial damage and loss. Outside the renal pelvis, inflammatory infiltrates were seen (Figure 2D).

Occasionally, in about 5% of *Mocos* KO mice, stones were found in the pelvis, sometimes leading to ureteral

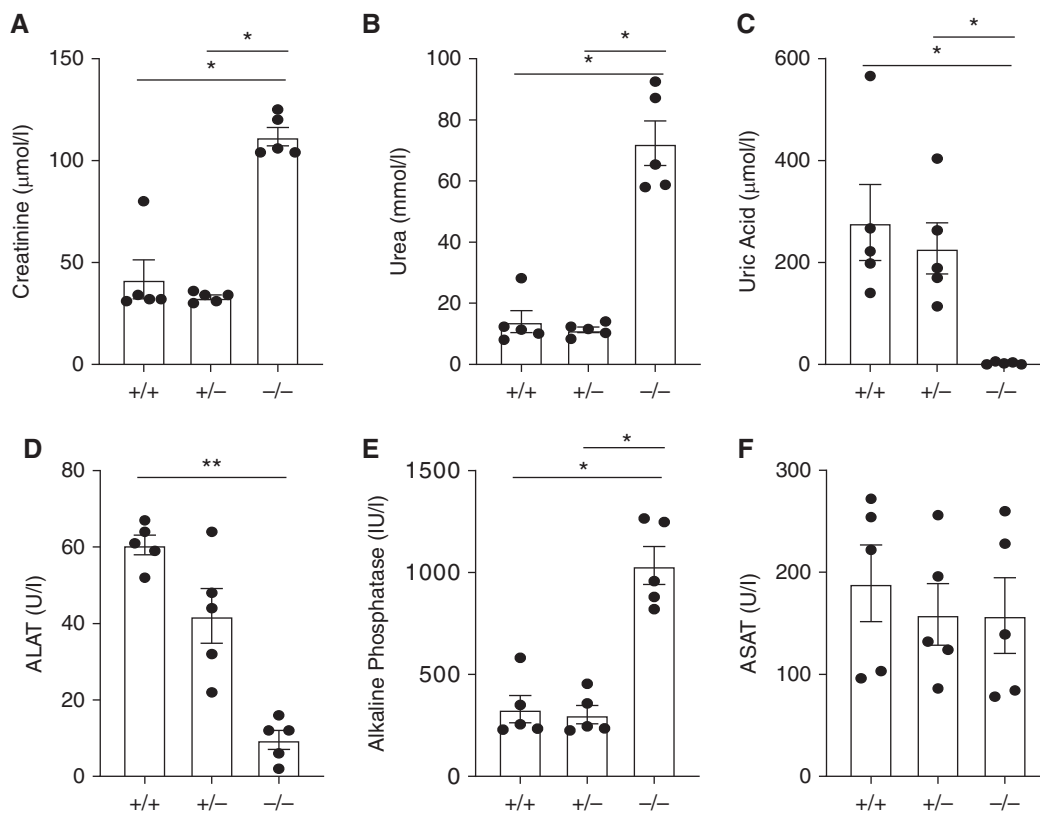


**Figure 4.** | Inactivation of *Mocos* leads to impaired renal and hepatic functions. Analysis of serologic parameters including (A) creatinine, (B) urea, (C) uric acid, (D) alanine aminotransferase (ALAT), (E) alkaline phosphatase, and (F) aspartate aminotransferase (ASAT) from 4-week-old animals. *Mocos*<sup>-/-</sup> mice were compared with heterozygous *Mocos*<sup>+/-</sup> and wild-type littermate controls ( $n=5$  for each genotype). Each bar represents the mean  $\pm$  SEM. ALAT, alanine aminotransferase; ASAT, aspartate aminotransferase. \* $P<0.05$ , \*\* $P<0.01$ .

obstruction. This obstruction was mostly unilateral and kidneys displayed a pale and swollen appearance. The histologic examination of these enlarged kidneys showed a uniformly thin, atrophic renal cortex and a marked dilation of the renal pelvis, characteristic of hydronephrosis (Supplemental Figure 2), whereas the contralateral kidney was small with obstructive nephropathy. Of note, heterozygous mice with partial loss of *Mocos* expression did not show a disturbed histology of other organs in young mice or in adult mice (Supplemental Figure 3).

#### Inactivation of *Mocos* Induces Xanthinuria

Because stones, sometimes clearly visible to the naked eye and large enough to interfere with normal urinary function, were frequently observed in urine and kidneys from affected *Mocos* mice (Figure 3A), we next analyzed the effects of urinary tract obstruction in biologic fluids. Consistent with a role of *Mocos* in purine metabolism, the colorless and acidic urine (Figure 3B), but also the serum collected from *Mocos*<sup>-/-</sup> mice, had high levels of xanthine and hypoxanthine as compared with age-matched controls (Figure 3, C and D). Kidney stones were composed of xanthine based on their unique Raman spectral fingerprints (Figure 3, E and F). The present morphologic and biochemical data thus strongly suggest that accumulation of xanthine crystals leads to intra- and extrarenal obstructive nephropathy in *Mocos* KO mice. Xanthine stones with

hydronephrosis are found in mice and in hereditary xanthinuria type II in humans, which is typically crystallopathy, but the prevailing feature in the *Mocos* KO mouse model is an obstructive nephropathy.

#### Renal Failure in *Mocos* KO Mice

Kidney dysfunction in *Mocos*-deficient mice was further evaluated by monitoring biochemical markers for the diagnosis of the progression of kidney damage. Our data denote profound metabolic changes, including drastic increases of serum creatinine and urea in *Mocos*<sup>-/-</sup> mice when compared to controls (Figure 4, A and B). As expected from the essential role of *Mocos* in XDH activity, *Mocos* KO mice had an almost undetectable level of uric acid (Figure 4C). In addition, the serum levels of some hepatic enzymes were altered, with a reduced level of alanine aminotransferase and an increased level of alkaline phosphatase in *Mocos*-deficient mice (Figure 4, D–F), which were not observed in heterozygous *Mocos* animals when compared to wild-type mice at 4 weeks of age or later in adult mice (Supplemental Figure 4, A–F). Altogether, these data suggest the physiopathologic changes produced by the complete inactivation of *Mocos* caused acute renal failure.

#### *Mocos* KO Mice Display Anemia

Because hematologic parameters are tightly regulated traits with high clinical relevance, we also analyzed the

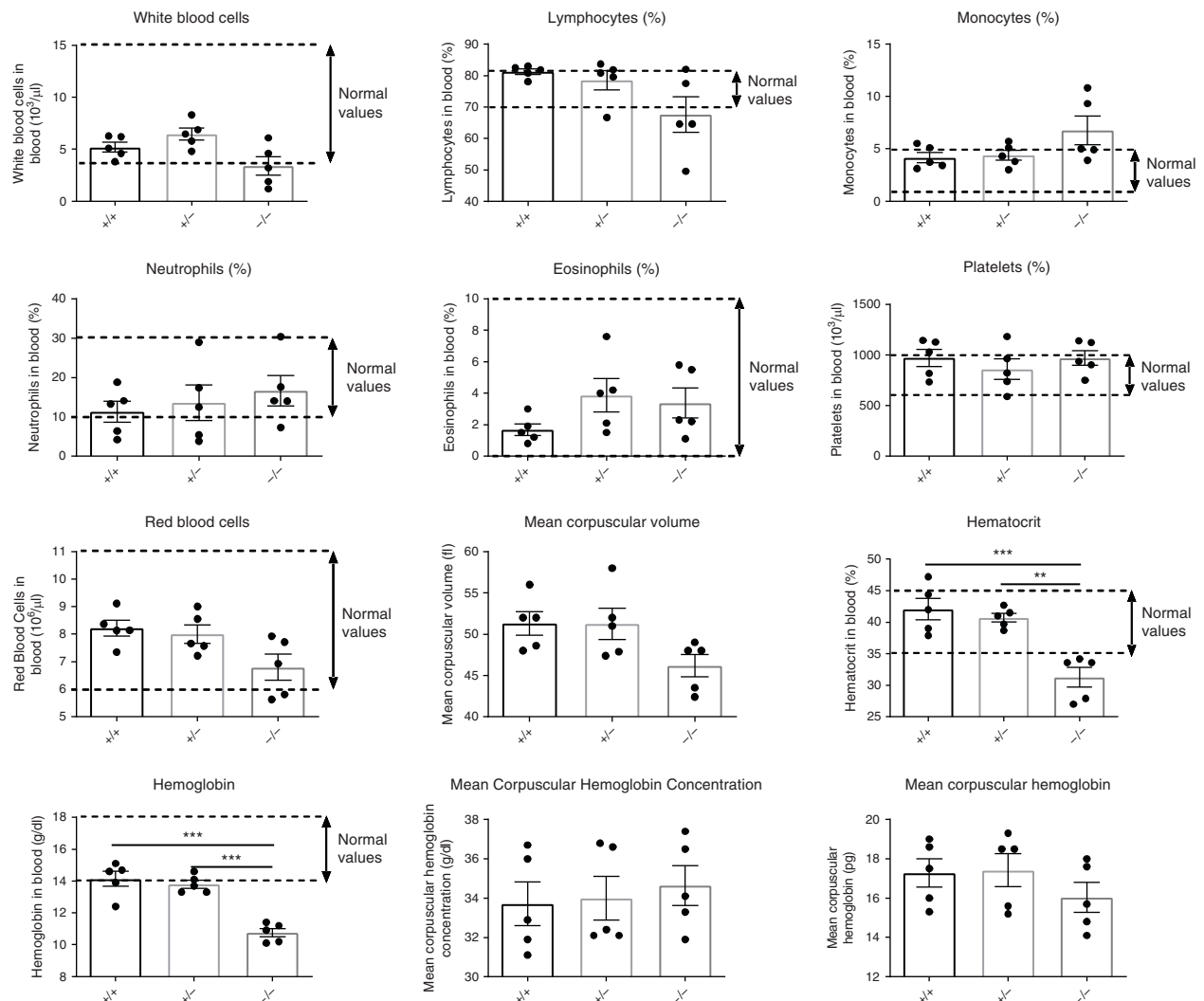


**Figure 5.** | *Mocos*<sup>-/-</sup> mice display anemia. White blood cell counts and differential counts performed to identify the type of leukocytes are given as a percentage. The hematogram of homozygous *Mocos*<sup>-/-</sup> mice was compared with that of littermate controls at 4 weeks of age. The reference range for each group of parameter is indicated. Data are expressed as mean ± SEM. \*\**P* < 0.01, \*\*\**P* < 0.001.

hematogram of *Mocos*<sup>-/-</sup> and control mice. When compared with littermate controls, *Mocos* KO mice tend to have almost normal distribution of total white blood cell counts (Figure 5). The differential cell counts to identify leukocytes were within the normal range, as was the number of platelets. This result excluded systemic inflammation, but also underscored the presence of mild anemia, with reduced circulating red blood cells and red cell parameter values outside normal ranges. Of note, hemoglobin and hematocrit values in *Mocos*<sup>-/-</sup> mice were significantly decreased compared with those in wild-type mice (Figure 5). These disturbances, accompanied by normal values of mean corpuscular volume and mean corpuscular hemoglobin concentration, were suggestive of normocytic anemia, a feature frequently associated with poor outcomes in acute and chronic renal failure (26). On the contrary, heterozygous *Mocos* mice showed normal hematologic parameters at 4 weeks of age and even later (Supplemental Figure 5).

### ***Mocos* KO Mice Display Increased Expression of Adipogenesis-Related Genes and Markers of Inflammation and Fibrosis**

We further investigated dysregulation of lipid metabolism and found enhanced expression of two important regulators of lipid homeostasis, namely CCAAT/enhancer-binding protein- $\beta$  and peroxisome proliferator activated receptor- $\gamma$  (PPAR $\gamma$ ) in *Mocos* KO mice compared with age-matched counterparts (Figure 6A). This altered lipid signaling network could contribute to the pathophysiology of xanthinuria and interfere with immune regulation because we observed a marked increase in mRNA expression of the proinflammatory factors TNF- $\alpha$  and monocyte chemoattractant protein 1 (Figure 6B). Finally, the significant activation of TGF- $\beta$ 1, which may contribute to renal interstitial fibrosis (27,28), and serpine 1, the main suppressor of the fibrinolytic system, suggests a vicious cycle of immune-metabolic dysregulation that could promote renal fibrotic



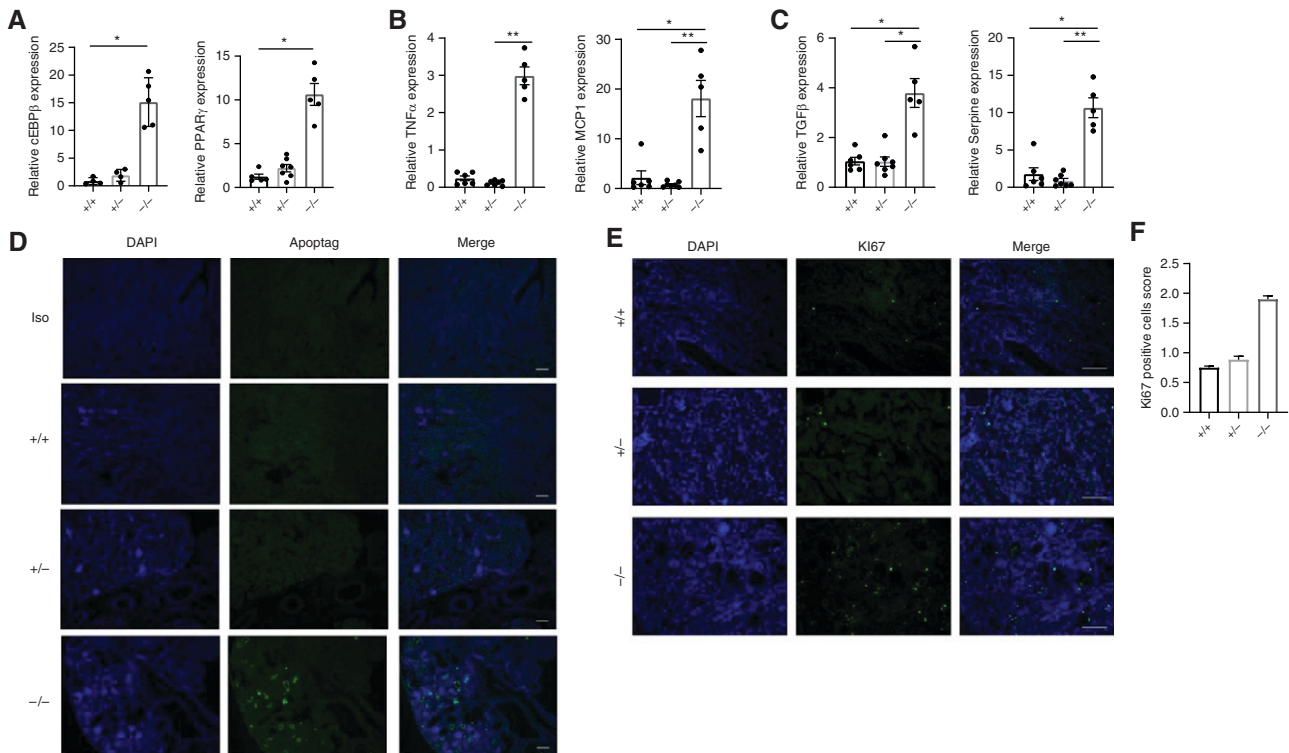


**Figure 6. | *Mocos* gene disruption induces expression of adipogenesis-related genes, inflammatory response, and interstitial fibrosis in *Mocos*<sup>-/-</sup> kidney.** (A) Enhanced expression of C/EBP-β and PPARγ in *Mocos* KO mice compared with controls. Transcription was measured by real-time PCR (RT-PCR) in 4-week-old mice. Data are expressed as mean±SEM. (B) Genes involved in the inflammatory response were significantly upregulated in *Mocos* KO kidneys when compared with kidneys from littermate controls. Expression levels of TNF-α and MCP1/CCL2 were measured by RT-PCR. Data were from mice at 4 weeks of age and are expressed as mean±SEM. (C) Disruption of the *Mocos* gene–induced renal interstitial fibrosis. The expression levels of TGF-β1 and serpine/PAI1 were measured by RT-PCR in 4-week-old mice ( $n=5$  for each genotype). Results are expressed as mean±SEM. (D) Terminal deoxynucleotidyl transferase–mediated digoxigenin–deoxyuridine nick-end labeling staining shows apoptosis of tubular epithelial cells in kidneys from *Mocos*<sup>-/-</sup> mice. Scale bar, 100 μm. (E) Immunofluorescence staining of Ki67 revealed markedly increased cell proliferation in kidneys of *Mocos* KO mice at 4 weeks of age when compared with controls. 4',6-Diamidino-2-phenylindole (DAPI) was used to label nuclei. (F) Quantitation of cell proliferation was determined by counting the number of Ki67-positive nuclei in each mouse strain of the specified genotypes. RT-PCR, real-time PCR; DAPI, 4',6-Diamidino-2-phenylindole. \* $P<0.05$ , \*\* $P<0.01$ .

responses and kidney dysfunction in *Mocos*<sup>-/-</sup> kidneys (Figure 6C). Immunofluorescence imaging ultimately supported visual evidence for tubular damage and repair, with increased ApoptTag staining (Figure 6D) accompanied by increased fluorescence signal of the proliferating cell marker Ki67 in *Mocos*<sup>-/-</sup> kidneys (Figure 6, E and F). No sign of inflammation or fibrosis was detected in kidneys of heterozygous *Mocos* and wild-type littermates at 4 weeks of age.

### Impaired Ability of Xanthinuric Animals to Mount the Biologic Response to Overcome Oxidative Stress and Inflammation

Because PPARγ plays additional roles by participating in inflammation and oxidative stress in renal disease, we next examined redox homeostasis in *Mocos*<sup>-/-</sup> mice. Further confirming the potential antioxidative protective effect of PPARγ (Figure 6A) (29), we found that NOX4, a NADPH oxidase isoform expressed in proximal tubular cells and known to be an important source of ROS (30), was significantly underexpressed in *Mocos*<sup>-/-</sup> kidney when compared with littermate controls (Figure 7A). These possible renoprotective effects of NOX4 and PPARγ were accompanied by

increased expression of glutamate-cysteine ligase (the key enzyme in glutathione synthesis), but impaired activation of genes encoding many antioxidant and detoxifying enzymes known to be targets of PPARγ and Nrf2 (Figure 7, B–F). Particularly noteworthy was the dysregulation of the thioredoxin (TXN)-based antioxidant system, with the significant increase of TXN-inhibitory protein and TXN-domain containing 12, which suggested a disruption of the TXN-inhibitory protein–TXN complex and endoplasmic reticulum stress in *Mocos*<sup>-/-</sup> kidneys (Figure 7, G–I, and Wu *et al.* [31]). Finally, our data highlighted the importance of reactive carbonyl species stress in affected *Mocos*<sup>-/-</sup> kidneys expressing aberrant levels of AKR1B8 and AKR1C1, two members of the aldo-keto reductase superfamily involved in detoxification of cytotoxic carbonyls and balance of electrolytes and potassium, respectively (Figure 7, J and K).

### Major Dysfunctions of Purine, Amino Acid, and Phospholipid Pathways in Kidneys from Xanthinuric *Mocos* Mice

A metabolomics approach was next performed using liquid chromatography tandem high-resolution mass spectrometry to uncover altered metabolites and biologic

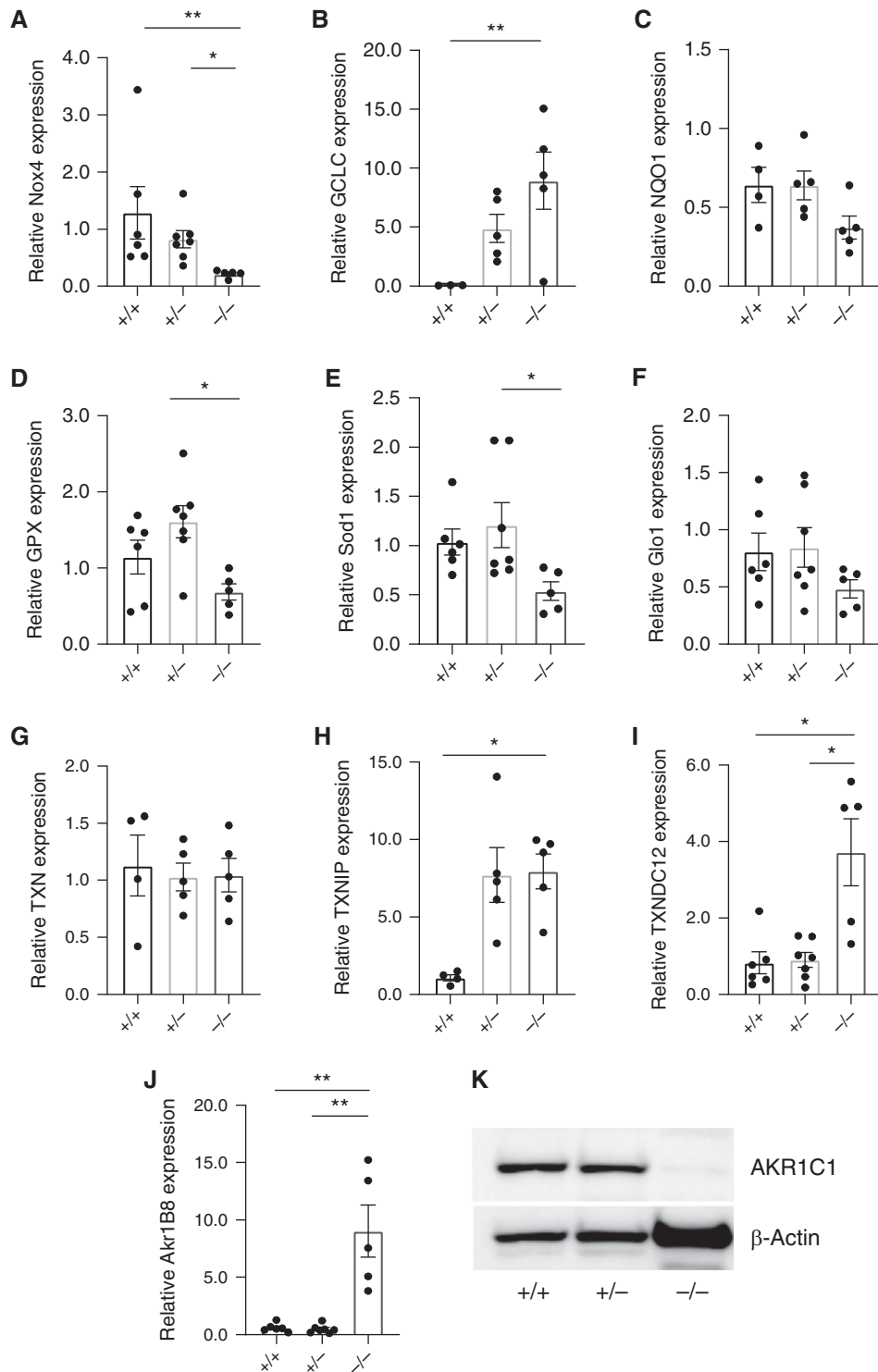


**Figure 7. | *Mocos* deletion alters detoxification defenses in kidney.** (A) Disruption of *Mocos* induces decreased expression levels of NADPH oxidase 4 (NOX4) and (B) increased transcription of glutamate-cysteine ligase catalytic subunit (GCLC) but no modification of genes encoding several antioxidant and detoxifying enzymes such as (C) NADPH(H) quinone dehydrogenase 1 (NQO1), (D) glutathione peroxidase 1 (GPX1), (E) superoxide dismutase 1 (SOD1), and (F) glyoxalase 1 (GLO1) in *Mocos*<sup>-/-</sup> kidneys when compared to littermate controls. (G–H) The transcription of thioredoxin (TXN) was not affected but the TXN complex was unbalanced, with significant upregulation of TXN-inhibitory protein (TXNIP) in xanthinuric mice. (I) Expression of TXN-domain containing 12 (TXNDC12) dithiol-disulfide oxidoreductase of the endoplasmic reticulum and (J) AKR1B8, an aldoketoreductase involved in carbonyl detoxification, was significantly upregulated in *Mocos*<sup>-/-</sup> mice but not in wild-type and heterozygous mice. All results were obtained by real-time PCR in kidneys of 4-week-old mice ( $n=4-7$  for each genotype). Results were expressed as mean  $\pm$  SEM. (K) Renal expression of AKR1C1 is significantly disturbed in *Mocos* KO mice when compared with controls (Western blot). NOX4, NADPH oxidase 4; GCLC, glutamate-cysteine ligase catalytic subunit; NQO1, NADPH(H) quinone dehydrogenase 1; GPX1, glutathione peroxidase 1; SOD1, superoxide dismutase 1; GLO1, glyoxalase 1; TXN, thioredoxin; TXNIP, TXN-inhibitory protein; TXNDC12, TXN-domain containing 12. \* $P<0.05$ , \*\* $P<0.01$ .

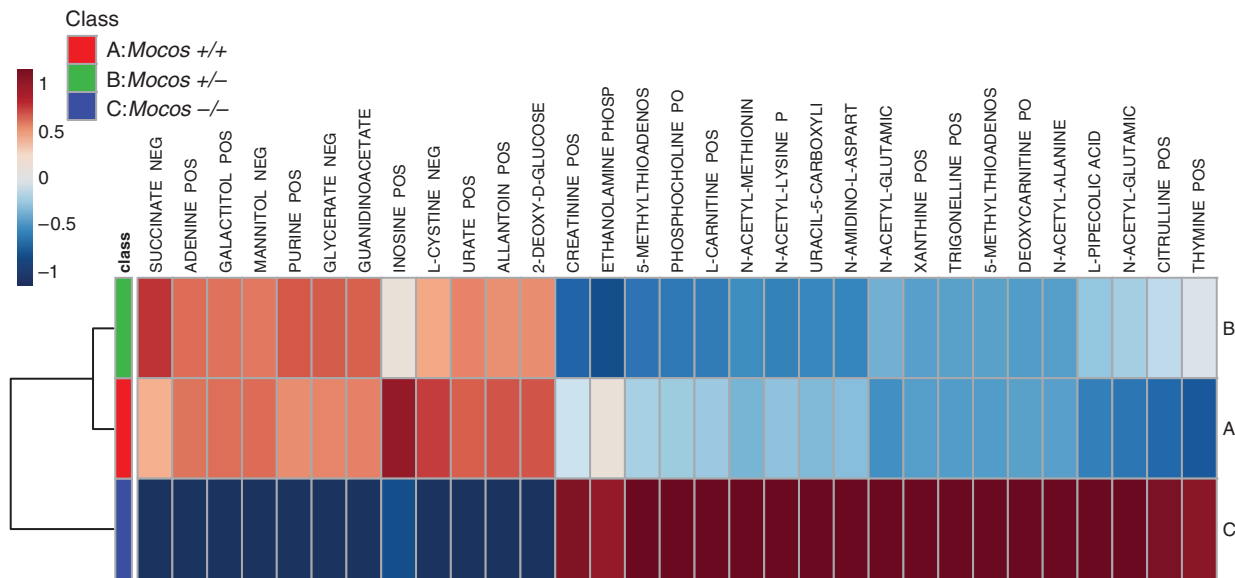


**Figure 8. | Purines, amino acids and phospholipids metabolic pathways are altered in *Mocos* knockout kidneys.** Heat map depicting the top 31 most significantly affected metabolites, where red indicates an increase in concentration and blue indicates a decrease. Kidneys from young *Mocos*<sup>-/-</sup> mice (class C) were compared with kidneys from *Mocos*<sup>+/-</sup> (class B) and wild-type littermates (class A). Euclidian distance used for measuring distance, and Ward method used as the clustering algorithm. NEG, negative; POS, positive.

pathways in *Mocos*<sup>-/-</sup> kidneys. As illustrated in Figure 8 and Supplementary Table 1, no significant modification of metabolites was observed in kidney tissues from *Mocos*<sup>+/-</sup> mice compared with wild-type mice. Conversely, *Mocos*<sup>-/-</sup> kidneys revealed significant metabolic perturbations: of the 121 robust metabolites analyzed, 40 metabolites were altered when compared with wild-type mice, and 31 metabolites showed perturbation of renal expression when the three *Mocos*<sup>+/+</sup>, *Mocos*<sup>+/-</sup>, and *Mocos*<sup>-/-</sup> kidney groups were compared (Figure 8 and Supplemental Figure 6). As expected, lack of MOCOS activity resulted in very low levels of uric acid and allantoin, the primary product of urate oxidation (Figure 8). In this pathway, xanthine and its distant precursors, such as inosine and adenine, were also affected. This result thus reinforced the finding that the main metabolic function of *Mocos* is restrained to the purine catabolism pathway. In parallel, in agreement with the role of *Mocos* in a physiologic alternative to the “classic” pathway of NO formation from L-arginine, the integrity of the arginine-NO/urea system was

also disturbed in *Mocos*<sup>-/-</sup> kidneys, with a strong perturbation of citrulline and guanidoacetic acid (a precursor of creatine), two known metabolites of the urea cycle (Table 1). Interestingly, Table 1 also highlights significantly altered metabolites involved in energy metabolism and mitochondrial function, such as trimethylammonio butanoic acid, whereas the decreased cysteine metabolism might further denote oxidative damage in *Mocos* KO kidneys. Finally, other notably disturbed metabolic pathways include the phospholipid biosynthetic pathway, indicative of massive membrane remodeling of renal cells, and the serotonin pathway (5-hydroxyindole acetate), indicative of tryptophan metabolism (Figure 8, Table 1, and Supplemental Table 2).

In summary, the metabolic analysis of *Mocos*<sup>-/-</sup> kidneys underscored the essential role of purines and highlighted the potential pathophysiologic implications of the deregulation of amino acids (three pathways) and phospholipids metabolisms (two pathways) in kidneys of *Mocos*-deficient mice (Supplemental Figure 7).

**Table 1. List of the top six main disturbed pathways, and the related dysregulated metabolites, in kidneys from the three groups of mice (*Mocos*<sup>+/+</sup>, *Mocos*<sup>+/-</sup>, and *Mocos*<sup>-/-</sup> mice)**

Pathway Name	Matched Metabolites
Arginine and proline metabolism	Citrulline, guanidoacetic acid, N-acetyl-L-alanine, 4-guanidinobutanoic acid
Purine metabolism	Xanthine, inosine, uric acid, adenine
Lysine degradation	4-Trimethylammonio butanoic acid, pipecolic acid
Cysteine and methionine metabolism	5'-Methylthioadenosine, L-cystine
Glycerophospholipid metabolism	Phosphorylcholine, O-phosphoethanolamine
Glycine, serine, and threonine metabolism	Glyceric acid, guanidoacetic acid
<i>Mocos</i> , molybdenum cofactor sulfurase.	

## Discussion

Xanthinuria is an under-recognized disorder that, in less than half of affected individuals, is characterized by xanthine stones. This rare genetic disorder may be accompanied by hydronephrosis and, eventually, other complications of urolithiasis, such as pyelonephritis. In our *Mocos*-deficient mouse model of xanthinuria, the leading pathology is obstructive nephropathy. To our knowledge, such a pathology has not been reported in either type I or type II xanthinuria in humans. Nonetheless, the *Mocos* mouse may serve as a model to study the pathogenesis of obstructive nephropathy. Remarkably, the signs of obstructive nephropathy found in *Mocos* KO mice do not differ from those reported in humans affected by other forms of obstructive nephropathies of variable etiology, such as nephrocalcinosis after hyperphosphaturia or hypercalciuria, calcium oxalate nephropathy, urate nephropathy, myeloma kidney, or obstruction due to drug crystals (32). Recently, an attempt to classify crystal nephropathies was proposed according to the localization of crystal deposits in the renal vasculature (type 1), the nephron (type 2), or the draining urinary tract (type 3) (33). Regarding this classification, analysis of the morphologic data of *Mocos*-deficient mice suggests a prevalence of type 2 and a minor contribution of type 3 nephropathy.

The mechanisms of xanthine crystal precipitation are not resolved but may involve neutrophils, interstitial and tubular inflammation with inflammatory cytokines, together with precipitation of THPs. Different crystals cause injury in numerous disorders and induce inflammation *via* the NLRP3 inflammasome and cell death (34). Mulay *et al.* (34) found that crystals of calcium oxalate, monosodium urate, calcium pyrophosphate dihydrate, and cystine may trigger caspase-independent cell death *via* TNF- $\alpha$ /TNFR1, RIPK1, RIPK3, and MLKL, and initiate tissue injury and organ failure. However, tissue damage and inflammation induced by xanthine crystals have not been reported so far. In view of the tubular cell necrosis and interstitial inflammation in *Mocos* KO mice, activation of the inflammasome or other danger signal pathways are likely activated, causing inflammation. These pathways, including DNA sensing pathways, need further investigation to understand the molecular mechanisms behind the cellular processes that contribute to the onset and development of the disease. To explain how *Mocos* deletion may cause xanthinuria type II, we suggest a two-step process involving (1) an obstructive nephropathy due to production, poor solubility, and intratubular precipitation of xanthine; and (2) cell stress and death mediated by altered detoxification circuitry, impairment of nutrient delivery, and waste product removal from kidney cells. The cellular stress elicited by these events causes inflammation triggering crystal formation, which may then enhance renal pathology.

In the *Mocos*-deficient mouse model of obstructive nephropathy, renal stones and decreased renal function are associated with hypouricemia and altered detoxification circuitry. Whereas xanthine stones may be proinflammatory and worsen renal function, several studies have reported positive correlations between hyperuricemia, kidney inflammation, and renal failure induced by urate crystal formation (35,36). However, hypouricemia caused by

increased excretion or diminished reabsorption of filtered uric acid is also observed in humans (37), and it is established that uric acid is the most abundant soluble antioxidant preserving endothelial function in situations of oxidative stress (38). Inflammation and oxidative stress are known to be involved in the pathogenesis of CKD in humans and in chronic renal failure in animal models. As far as kidney stone disease is concerned, particularly calcium oxalate, injury induced by high concentrations of oxalate in renal tubular epithelial cells is related to oxidative stress, tissue inflammation, and mitochondrial dysfunction (39). Our data show disruption of intrarenal redox homeostasis and are consistent with the essential role of MOCOS in aldehyde detoxification (19,20) and the relevance of reactive carbonyl species metabolism in ROS-related renal injury (40,41). These data point to the poor ability of xanthinuric animals to mount a protective response to overcome oxidative stress *via* inflammation.

Metabolomics studies allowed the differential diagnosis of type I and type II classic xanthinuria. These studies have highlighted the role of the purine degradation pathway but also pathways involved in amino acid metabolism (such as tryptophan), vitamin B6, nicotinamide, and possibly polyamine catabolism in patients with xanthinuria type II. Severe symptoms are rarely observed in patients with classic xanthinuria; usually they present with mild symptoms. Despite conservation of purine metabolism, the significant differences between mice and humans likely reflect divergent features of key stages of kidney development. Moreover, the level of uric acid in mice is lower than that in humans because uricase, an enzyme present in mouse but not in humans, degrades uric acid into allantoin. Thus, decreased XDH and uric acid levels in the immediate postnatal period in *Mocos*-deficient mice may significantly affect renal development and amplify xanthinuria. Although neonatal *Mocos* KO mice cannot overcome MOCOS deficiency, we assume that the 50% reduction of MOCOS expression in heterozygous mice might be sufficient for a normal renal and metabolic function in young and aged mice.

Beside its role in nephropathology, MOCOS is involved in complex disorders, such as ASD (20–22). Although metabolomic studies on complex disorders are far from definitive and unambiguous, analysis of the metabolome has shown great potential to uncover biomarkers for complex diseases such as ASD. Indeed, recent studies on urine from patients with ASD have reported that several metabolic profiles associated with amino acids, purine metabolism, creatine metabolism, energy metabolism, and oxidative stress could be involved in ASD (42,43).

In conclusion, the *Mocos* mouse model may enable an integrated understanding of xanthinuric obstructive nephropathy and of common mechanisms underlying complex diseases, such as metabolic disorders and ASD.

## Disclosures

All authors have nothing to disclose.

## Funding

This work was supported by Centre National de la Recherche Scientifique (CNRS), Institut National de la Santé et de la Recherche Médicale (INSERM), University of Orléans, University



of Tours, and the European funding in Region Centre-Val de Loire (FEDER N°2016-00110366=BIO-TARGET 2015-2018 and FEDER N°EX005756=BIO-TARGETII).

### Acknowledgments

We would like to thank PHENOMIN and ICS for the generation of *Mocos* KO mice. Our special thanks go to Dr. François Erard for critical review of the manuscript, Melody Thilloux and Mathilde Favrat for technical assistance and animal handling. We are also grateful to TAAM and, more specifically, to Emilie Bouvier and Severine Grieszmann for taking care of the animals. We also thank the department Analyse des Systemes Biologiques (PST ASB, Université de Tours, France) for their help with sample analyses.

### Author Contributions

M. Erard-Garcia, conceptualized the study; E. Culerier, A. Dudas, N. Erard, M. Erard-Garcia, F. Foucher, M. Le Bert, A. Lefevre, C. Mackowiak, S. Mavel, M.J. Mihatsch, J. Pailloux, P. Rontani, and D. Sedda were responsible for investigation; P. Emond, M. Erard-Garcia, F. Foucher, C. Mackowiak, S. Mavel, and M.J. Mihatsch were responsible for data curation; P. Emond, M. Erard-Garcia, C. Mackowiak, S. Mavel, M.J. Mihatsch and B. Ryffel were responsible for formal analysis; M. Erard-Garcia provided supervision and was responsible for validation; M. Erard-Garcia, M.J. Mihatsch, and B. Ryffel wrote the original draft and reviewed and edited the manuscript; M. Erard-Garcia and B. Ryffel were responsible for project administration; and V.F.J. Quesniaux was responsible for funding acquisition.

### Supplemental Material

This article contains the following supplemental material online at <http://kidney360.asnjournals.org/lookup/suppl/doi:10.34067/KID.0001732021/-/DCSupplemental>.

Supplemental Appendix. Supplemental Methods.

Supplemental Figure 1. Heterozygous *Mocos* mice develop normally but *Mocos* KO mice display major morphologic abnormalities in kidney, liver and brain.

Supplemental Figure 2. Deletion of *Mocos* causes occasional hydronephrosis in homozygous mutants surviving until 2 months.

Supplemental Figure 3. *Mocos* disruption does not change the histology of organs except the kidney in young mice.

Supplemental Figure 4. Adult heterozygous *Mocos* mice display no disturbances of renal function.

Supplemental Figure 5. Adult heterozygous *Mocos* mice exhibit normal hematological parameters.

Supplemental Figure 6. Clustering result shown as heatmap for the discriminant metabolites in kidney from the 3 groups of *Mocos*<sup>+/+</sup>, *Mocos*<sup>+/-</sup> and *Mocos*<sup>-/-</sup> mice.

Supplemental Figure 7. The purine and arginine/nitric oxide pathways in xanthinuric mice.

Supplemental Table 1. List of primers.

Supplemental Table 2. Listing of discriminant metabolites obtained after univariate analysis.

### References

- Bradbury MG, Henderson M, Brocklebank JT, Simmonds HA: Acute renal failure due to xanthine stones. *Pediatr Nephrol* 9: 476–477, 1995 <https://doi.org/10.1007/BF008667327577413>
- Chalmers RA, Watts RW, Pallis C, Bitensky L, Chayen J: Crystalline deposits in striped muscle in xanthinuria. *Nature* 221: 170–171, 1969 <https://doi.org/10.1038/221170a05782709>
- Pacher P, Nivorozhkin A, Szabó C: Therapeutic effects of xanthine oxidase inhibitors: Renaissance half a century after the discovery of allopurinol. *Pharmacol Rev* 58: 87–114, 2006 <https://doi.org/10.1124/pr.58.1.616507884>
- Ichida K, Matsumura T, Sakuma R, Hosoya T, Nishino T: Mutation of human molybdenum cofactor sulfurase gene is responsible for classical xanthinuria type II. *Biochem Biophys Res Commun* 282: 1194–1200, 2001 <https://doi.org/10.1006/bbrc.2001.471911302742>
- Yamamoto T, Moriwaki Y, Takahashi S, Tsutsumi Z, Tuneyoshi K, Matsui K, Cheng J, Hada T: Identification of a new point mutation in the human molybdenum cofactor sulfurase gene that is responsible for xanthinuria type II. *Metabolism* 52: 1501–1504, 2003 [https://doi.org/10.1016/S0026-0495\(03\)00272-514624414](https://doi.org/10.1016/S0026-0495(03)00272-514624414)
- Peretz H, Naamati MS, Levartovsky D, Lagziel A, Shani E, Horn I, Shalev H, Landau D: Identification and characterization of the first mutation (Arg776Cys) in the C-terminal domain of the Human Molybdenum Cofactor Sulfurase (HMCS) associated with type II classical xanthinuria. *Mol Genet Metab* 91: 23–29, 2007 <https://doi.org/10.1016/j.ymgme.2007.02.00517368066>
- Watanabe T, Ihara N, Itoh T, Fujita T, Sugimoto Y: Deletion mutation in *Drosophila* ma-I homologous, putative molybdopterin cofactor sulfurase gene is associated with bovine xanthinuria type II. *J Biol Chem* 275: 21789–21792, 2000 <https://doi.org/10.1074/jbc.C00023020010801779>
- Zhou Y, Zhang X, Ding R, Li Z, Hong Q, Wang Y, Zheng W, Geng X, Fan M, Cai G, Chen X, Wu D: Using next-generation sequencing to identify a mutation in human MCSU that is responsible for type II xanthinuria. *Cell Physiol Biochem* 35: 2412–2421, 2015 <https://doi.org/10.1159/00037404225967871>
- Murgiano L, Jagannathan V, Piffer C, Diez-Prieto I, Bolcato M, Gentile A, Drögemüller C: A frameshift mutation in MOCOS is associated with familial renal syndrome (xanthinuria) in Tyrolean Grey cattle. *BMC Vet Res* 12: 276, 2016 <https://doi.org/10.1186/s12917-016-0904-427919260>
- Mayr SJ, Mendel RR, Schwarz G: Molybdenum cofactor biology, evolution and deficiency. *Biochim Biophys Acta Mol Cell Res* 1868: 118883, 2021 <https://doi.org/10.1016/j.bbamcr.2020.11888333017596>
- Anantharaman V, Aravind L: MOSC domains: ancient, predicted sulfur-carrier domains, present in diverse metal-sulfur cluster biosynthesis proteins including Molybdenum cofactor sulfurases. *FEMS Microbiol Lett* 207: 55–61, 2002 [https://doi.org/10.1016/S0378-1097\(01\)00515-811886751](https://doi.org/10.1016/S0378-1097(01)00515-811886751)
- Hille R, Hall J, Basu P: The mononuclear molybdenum enzymes. *Chem Rev* 114: 3963–4038, 2014 <https://doi.org/10.1021/cr400443z24467397>
- Bittner F: Molybdenum metabolism in plants and crosstalk to iron. *Front Plant Sci* 5: 28, 2014 <https://doi.org/10.3389/fpls.2014.0002824570679>
- Battelli MG, Bortolotti M, Polito L, Bolognesi A: The role of xanthine oxidoreductase and uric acid in metabolic syndrome. *Biochim Biophys Acta Mol Basis Dis* 1864: 2557–2565, 2018 <https://doi.org/10.1016/j.bbadis.2018.05.00329733945>
- Ichida K, Amaya Y, Okamoto K, Nishino T: Mutations associated with functional disorder of xanthine oxidoreductase and hereditary xanthinuria in humans. *Int J Mol Sci* 13: 15475–15495, 2012 <https://doi.org/10.3390/ijms13111547523203137>
- Ives A, Nomura J, Martinon F, Roger T, LeRoy D, Miner JN, Simon G, Busso N, So A: Xanthine oxidoreductase regulates macrophage IL1 $\beta$  secretion upon NLRP3 inflammasome activation. *Nat Commun* 6: 6555, 2015 <https://doi.org/10.1038/ncomms755525800347>
- Terao M, Romão MJ, Leimkühler S, Bolis M, Fratelli M, Coelho C, Santos-Silva T, Garattini E: Structure and function of mammalian aldehyde oxidases. *Arch Toxicol* 90: 753–780, 2016 <https://doi.org/10.1007/s00204-016-1683-126920149>
- Kundu TK, Velayutham M, Zweier JL: Aldehyde oxidase functions as a superoxide generating NADH oxidase: An important redox regulated pathway of cellular oxygen radical formation. *Biochemistry* 51: 2930–2939, 2012 <https://doi.org/10.1021/bi300087922404107>
- Terao M, Garattini E, Romão MJ, Leimkühler S: Evolution, expression, and substrate specificities of aldehyde oxidase

- enzymes in eukaryotes. *J Biol Chem* 295: 5377–5389, 2020 <https://doi.org/10.1074/jbc.REV119.00774132144208>
20. Féron F, Gepner B, Lacassagne E, Stephan D, Mesnage B, Blanchard MP, Boulanger N, Tardif C, Deveze A, Rousseau S, Suzuki K, Izpisua Belmonte JC, Khrestchatsky M, Nivet E, Erard-Garcia M: Olfactory stem cells reveal MOCOS as a new player in autism spectrum disorders. *Mol Psychiatry* 21: 1215–1224, 2016 <https://doi.org/10.1038/mp.2015.10626239292>
  21. Taheri M, Noroozi R, Aghaei K, Omrani MD, Ghafouri-Fard S: The rs594445 in MOCOS gene is associated with risk of autism spectrum disorder. *Metab Brain Dis* 35: 497–501, 2020 <https://doi.org/10.1007/s11011-019-00524-y31900757>
  22. Rontani P, Perche O, Greetham L, Jullien N, Gepner B, Féron F, Nivet E, Erard-Garcia M: Impaired expression of the COS-MOC/MOCOS gene unit in ASD patient stem cells. *Mol Psychiatry* 26: 1606–1618, 2021 <https://doi.org/10.1038/s41380-020-0728-232327736>
  23. Diémé B, Lefèvre A, Nadal-Desbarats L, Galineau L, Madji Hounoum B, Montigny F, Blasco H, Andres CR, Emond P, Mavel S: Workflow methodology for rat brain metabolome exploration using NMR, LC-MS and GC-MS analytical platforms. *J Pharm Biomed Anal* 142: 270–278, 2017 <https://doi.org/10.1016/j.jpba.2017.03.06828531831>
  24. Lefèvre A, Mavel S, Nadal-Desbarats L, Galineau L, Attucci S, Dufour D, Sokol H, Emond P: Validation of a global quantitative analysis methodology of tryptophan metabolites in mice using LC-MS. *Talanta* 195: 593–598, 2019 <https://doi.org/10.1016/j.talanta.2018.11.09430625588>
  25. Xia J, Wishart DS: Using metaboanalyst 3.0 for comprehensive metabolomics data analysis. *Curr Protoc Bioinformatics* 55: 14.10.1–14.10.91, 2016
  26. Babitt JL, Lin HY: Mechanisms of anemia in CKD. *J Am Soc Nephrol* 23: 1631–1634, 2012 <https://doi.org/10.1681/ASN.201111107822935483>
  27. Meng XM, Nikolic-Paterson DJ, Lan HY: TGF- $\beta$ : The master regulator of fibrosis. *Nat Rev Nephrol* 12: 325–338, 2016 <https://doi.org/10.1038/nrneph.2016.4827108839>
  28. Humphreys BD: Mechanisms of renal fibrosis. *Annu Rev Physiol* 80: 309–326, 2018 <https://doi.org/10.1146/annurev-physiol-022516-03422729068765>
  29. Ma Y, Shi M, Wang Y, Liu J: PPAR $\gamma$  and its agonists in chronic kidney disease. *Int J Nephrol* 2020: 2917474, 2020 <https://doi.org/10.1155/2020/291747432158560>
  30. Gorin Y: The kidney: An organ in the front line of oxidative stress-associated pathologies. *Antioxid Redox Signal* 25: 639–641, 2016 <https://doi.org/10.1089/ars.2016.680427357313>
  31. Wu M, Li R, Hou Y, Song S, Han W, Chen N, Du Y, Ren Y, Shi Y: Thioredoxin-interacting protein deficiency ameliorates kidney inflammation and fibrosis in mice with unilateral ureteral obstruction. *Lab Invest* 98: 1211–1224, 2018 <https://doi.org/10.1038/s41374-018-0078-829884908>
  32. Khan SR, Pearle MS, Robertson WG, Gambaro G, Canales BK, Doizi S, Traxer O, Tiselius HG: Kidney stones. *Nat Rev Dis Primers* 2: 16008, 2016 <https://doi.org/10.1038/nrdp.2016.827188687>
  33. Mulay SR, Anders HJ: Crystal nephropathies: Mechanisms of crystal-induced kidney injury. *Nat Rev Nephrol* 13: 226–240, 2017 <https://doi.org/10.1038/nrneph.2017.1028218266>
  34. Mualy SC, Kulkarni OP, Rupanagudi KV, Migliorini A, Darisipudi MN, Vilaysane A, Muruve D, Shi Y, Munro F, Liapis H, Anders H-J: Calcium oxalate crystals induce renal inflammation by NLRP3-mediated IL-1 $\beta$  secretion. *J Clin Invest* 123: 236–246, 2013 <https://doi.org/10.1172/JCI63679>
  35. Kang DH, Nakagawa T, Feng L, Watanabe S, Han L, Mazzali M, Truong L, Harris R, Johnson RJ: A role for uric acid in the progression of renal disease. *J Am Soc Nephrol* 13: 2888–2897, 2002 <https://doi.org/10.1097/01.ASN.0000034910.58454.FD12444207>
  36. Mihai S, Codrici E, Popescu ID, Enciu AM, Albulescu L, Necula LG, Mambet C, Anton G, Tanase C: Inflammation-related mechanisms in chronic kidney disease prediction, progression, and outcome. *J Immunol Res* 2018: 2180373, 2018 <https://doi.org/10.1155/2018/218037330271792>
  37. Nishizaki N, Fujinaga S, Hirano D, Kanai H, Kaya H, Ohtomo Y, Shimizu T, Nozu K, Kaneko K: Hereditary renal hypouricemia: A cause of calcium oxalate urolithiasis in a young female. *Clin Nephrol* 77: 161–163, 2012 <https://doi.org/10.5414/CN10694922257548>
  38. Waring WS, McKnight JA, Webb DJ, Maxwell SR: Uric acid restores endothelial function in patients with type 1 diabetes and regular smokers. *Diabetes* 55: 3127–3132, 2006 <https://doi.org/10.2337/db06-028317065352>
  39. Tsuji H, Wang W, Sunil J, Shimizu N, Yoshimura K, Uemura H, Peck AB, Khan SR: Involvement of renin-angiotensin-aldosterone system in calcium oxalate crystal induced activation of NADPH oxidase and renal cell injury. *World J Urol* 34: 89–95, 2016 <https://doi.org/10.1007/s00345-015-1563-y25981400>
  40. Miyata T, Kurokawa K, van Ypersele de Strihou C: Relevance of oxidative and carbonyl stress to long-term uremic complications. *Kidney Int Suppl* 76: S120–S125, 2000 <https://doi.org/10.1046/j.1523-1755.2000.07615.x10936808>
  41. Ratliff BB, Abdulmahdi W, Pawar R, Wolin MS: Oxidant mechanisms in renal injury and disease. *Antioxid Redox Signal* 25: 119–146, 2016 <https://doi.org/10.1089/ars.2016.666526906267>
  42. Gevi F, Zolla L, Gabriele S, Persico AM: Urinary metabolomics of young Italian autistic children supports abnormal tryptophan and purine metabolism. *Mol Autism* 7: 47, 2016 <https://doi.org/10.1186/s13229-016-0109-527904735>
  43. Liu A, Zhou W, Qu L, He F, Wang H, Wang Y, Cai C, Li X, Zhou W, Wang M: Altered urinary amino acids in children with autism spectrum disorders. *Front Cell Neurosci* 13: 7, 2019 <https://doi.org/10.3389/fncel.2019.0000730733669>

**Received:** March 11, 2021 **Accepted:** September 13, 2021